**FZR-192**
September 1997

*R. Yanez*
*and the FOBOS collaboration*

# Pre- and post-scission
# light charged particle multiplicities
# in incomplete fusion reactions

# Pre- and post-scission light charged particle multiplicities in incomplete fusion reactions

## R. Yanez[1]
## and the FOBOS* collaboration

*Forschungszentrum Rossendorf, Instutut für Kern- und Hadronenphysik*
*Postfach 510119, D-01314 Dresden, Germany*

[1]*Present address: Indiana University Cyclotron Facility*
*2401 Milo B. Sampson Lane, Bloomington, IN 47408 USA*

**Abstract**
In this article we present results concerning the extraction of light charged particle multiplicities in incomplete fusion-fission reactions with a moving source fitting procedure. To demonstrate the feasibility and reliability of the procedure we have used simulated events of known multiplicity to construct kinetic energy distributions at different angles that are fitted assuming several pre- and post-scission sources. In particular, we show that it is necessary to include at least two pre-equilibrium sources in order to extract correctly the known pre-equilibrium proton multiplicity. These two sources are characterized by high emission temperatures, low emission barriers and high velocities, having $\sim 70\%$ and $\sim 25\%$ of the beam velocity along the beam axis, respectively. The former source is naturally dominant at forward angles due to the strong focusing effect of its high velocity. Contrary to normal expectations, however, the slower pre-equilibrium source is present with considerable yield at the most backward angles $\theta \sim 145°$ where it is normally assumed only evaporative components are present. The extracted proton multiplicities are well reproduced by the moving source procedure, as well as fitting parameters with physical relevance.

# I. INTRODUCTION

The nature and magnitude of nuclear viscosity and its effect on fission remain a topic of great interest. The dynamical retardation of fission due to the nuclear dissipation induced by viscosity is recognized through an increase of pre-scission particle emission, neutrons [1–3] and light charged particles [4], and the emission enhancement of giant dipole resonance (GDR) $\gamma$-rays [5,6], relative to predictions from standard statistical models. From these studies it now seems that nuclear dissipation is high when the fissioning system is sufficiently hot ($T \gtrsim 1.3$ MeV) and that the motion towards scission is strongly over-damped. The near constancy of the mean total kinetic energy (TKE) of fission fragments, for a given compound nucleus, with excitation energy, as evidenced by a well-known empirical relation [7], argues for such large overdamping in the collective motion towards fission, giving a rather modest radial kinetic energy contribution to the total energy.

The experimental and theoretical status is, however, rather controversial. Hinde et al. [3], for example, deduced a dynamical fission time scale of $(35\pm15)\times10^{-21}$ s by an analysis of pre-scission neutron multiplicities and mean kinetic energies in fusion-fission reactions leading to symmetric fission of compound nuclei with $A \sim 140 - 250$ and excitation energies $E^* \sim 0.3-1.2$ MeV/nucleon. Hinde also concluded that the dynamical time scale decreases with increasing mass asymmetry in the fission split. Similarly, Lestone [8] found a dynamical fission time scale of $(30 \pm 10) \times 10^{-21}$ s by analyzing pre-scission proton and $\alpha$-particle multiplicities and mean kinetic energies, also in fusion-fission reactions leading to the fission of compound nuclei with $A \sim 195$ and excitation energies $E^* \sim 0.3 - 0.5$ MeV/nucleon. The emission of light charged particles appear to be less sensitive to changes due to deformation of the emitting hot system and Lestone was therefore able to break-up the fission time scale into a pre-saddle $\tau_{pre}$ delay time and a saddle-to-scission $\tau_{ssc}$ transition time. Lestone's analysis is consistent with $\tau_{pre} = (9 \pm 6) \times 10^{-21}$ s and $\tau_{ssc} = (22 \pm 7) \times 10^{-21}$ s, implying that the hot system spends a considerable amount of time beyond the saddle point.

Time scales deduced from GDR $\gamma$-rays are in strong contradiction to those obtained using light particle multiplicities. Recently, to cite an example, van't Hof et al. [9] analyzed energy spectra of GDR $\gamma$-rays emitted form the compound nucleus $^{156}$Dy at excitations energies of $E^* \sim 0.7$ MeV/nucleon, and concluded that the fission time scale is of the order of $10^{-19}$ s and that the nuclear friction coefficient is in the range $0.01 < \gamma < 4$. It may be argued, however, that the transition time of a GDR $\gamma$-ray is typically given by the classical dipole sum rule $\sim 10^{-17}$ s (compared to emission times $\sim 10^{-22}$ to $10^{-21}$ s for light particles) and, therefore, the measuring scales are quite different. Adding to the controversy, Siwek-Wilczyñska et al. [10] concluded that the fission time scale is indeed of the order of $10^{-19}$ s when they confronted the neutron data of Hinde et al. [3] with simulations of a dynamical one-body dissipation model coupled to a time-dependent statistical model. In essence, their approach consist in regarding the evaporation cascade to take place during the fission process itself and, therefore, their results agree closely with the approach of reducing the standard fission decay width [11] with Kramers factor [12], used in most analyzes to reproduce GDR $\gamma$-ray multiplicities [6]. Furthermore, the analysis also concluded that the major contribution to the time scale comes from the time of formation of the excited nucleus to the time the system reaches the saddle point, in clear disagreement with Lestone's [8] conclusions.

Transient fission times deduced from light charged particle multiplicities are experimen-

tally not well established. Ikezoe et al. [13] measured and analyzed pre-scission proton and $\alpha$-particle multiplicities without any reference to nuclear dissipation whatsoever. The measured energy spectra and multiplicities could be fitted successfully with the standard statistical code PACE2 [14] using slightly reduced light-charged-particle emission barriers. The source of discrepancy could be that there is a rather sharp transition over a narrow range of excitation energy, below which no dissipation effects are present and standard statistical models describe the fission process correctly, and over which strong dissipation is needed to describe the experimental data [15]. Also, Moretto et al. [16] found no evidence for fission transient times in $\alpha$-particle induced fission reactions. The fission excitation functions of compound nuclei with $A = 186 - 213$ could be reproduced by taking into account shell corrections and using effective fission barriers. This suggests strong dynamical entrance-channel effects.

Despite the enormous increase of knowledge achieved in recent years, it is clear that several questions remain open. If dynamical fission delays related to nuclear dissipation along the collective motion towards scission appear to be a robust fact when the temperature is high enough, what remains to be determined is the magnitude and perhaps the tensorial nature of nuclear friction. Several theoretical studies have posed challenging questions to experimentalists. For example, in trying to simultaneously reproduce excitation functions and neutron multiplicities with calculations using a one-dimensional Langevin equation coupled to a statistical model, Fröbrich et al. [17] were lead to postulate a deformation dependent dissipation coefficient varying linearly form $\beta = 2 \times 10^{21}$ s$^{-1}$, where the necking in of the fissioning nucleus starts, to $\beta = 30 \times 10^{21}$ s$^{-1}$ at the scission point. Their success in accounting for neutron multiplicities and fission probabilities simultaneously argues for such a dependence. The temperature dependence of the dissipation coefficient inside the saddle point, with a $T$ or $T^2$ dependence, has also been postulated [15]. The temperature dependence tend to support a two-body dissipation mechanism, whereas the deformation dependence a one-body dissipation. Hence, the dissipation mechanism may start as two-body dissipation for compact shapes (compound nucleus) and turn over to a one-body dissipation mechanism for more deformed shapes (during the decent from saddle to scission point).

Up to now, the experimental efforts to extract fission time scales and nuclear friction coefficients have relied almost exclusively on the study of reactions where it is assumed the reacting nuclei fuse completely, forming fully equilibrated composite systems with relatively well-defined characteristics. In particular, the compound nuclei are formed with relatively moderate temperatures $T \sim 1.5 - 2.5$ MeV. To increase the temperature in a given system one would obviously need to increase the projectile energy. However, as the projectile energy increases, dynamical effects lead to an incomplete fusion mechanism in which particles or cluster of particles are emitted in the very early stages of the reaction, before the composite system reaches thermal equilibrium, carrying away considerable mass, energy, linear and angular momentum. Hence, an increase of excitation energy is achieved at the expense of a less defined composite nucleus. Also, the particles emitted before full thermal equilibration of the composite system, called pre-equilibrium particles, have to be disentangled from the particles emitted after thermalization, adding considerable complexity. The uncertainties in the properties of the composite system can be remedied by measuring both fission fragments and making reasonable assumptions about the relation between linear momentum transfer and excitation energy. This requirement calls for a high detection efficiency of such correlated pair of fragments achievable only in

$4\pi$ devices.

The $4\pi$ spectrometer FOBOS [18], located in Dubna, Russia, is one such device especially designed for the study of fission in reactions typically in the Fermi domain (20 $\lesssim E_{proj} \lesssim 60$ MeV/nucleon) where the reaction mechanism is characterized by the incomplete fusion of projectile and target. Its 30 detector modules cover nearly 60% of $4\pi$. Each module is able to deduce, event-by-event, the fission fragment masses, charges and momentum components in a broad dynamical range, by using position sensitive avalanche counters (PSAC) and Bragg-peak ionization chambers (BIC), and combining TOF$-E$ and $\Delta E - E$ techniques. A shell of CsI scintillator detectors positioned behind the fission fragment detectors are used to register independently coincident light charged particles. However, the high light charged particle detection threshold caused by the PSAC and BIC foils and gases, and distortions caused by thick supporting grids, does not permit a reliable extraction of multiplicities. Recently, a series of experiments were performed (36 MeV/nucleon $^{40}$Ar$+^{nat}$Ag,$^{232}$Th,$^{248}$Cm) in which the PSACs and BICs of three carefully selected modules were removed in order to record spectra without the above mentioned thresholds and distortions. This new data should permit an analysis aimed to extract of pre- and post-scission multiplicities in a regime of mass and temperature scarcely explored. The high geometrical efficiency of FOBOS and its ability to reconstruct the complete kinematics event-by-event induce great hopes of deducing the above quantities as a function of excitation energy of the composite system and mass asymmetry in the fission split. Since the post-scission multiplicities depend on the excitation energy left for the fragments at the moment of scission, the experimental data could provide valuable information about the excitation energy and its partition among the fragments at the moment of scission in very asymmetric mass splits. Awaiting experimental data we have performed realistic simulations of one of the reactions studied in the past by FOBOS, 53 MeV/nucleon $^{14}$N on $^{197}$Au. The composite system created in this reaction have masses $A \sim 197$ and temperatures $T \sim 4$ MeV. With the help of simulated events we construct energy distributions of light charged particles to test the feasibility and reliability of a moving source analysis to extract multiplicities in these reactions. How the analysis to extract light charged particle multiplicities, and the simulations to extract fission time scales and nuclear friction coefficients may be done is the topic of this article.

## II. SIMULATIONS

In order to construct energy distributions of particles, emitted prior or after fission takes place, we have coupled two models. The first is the Boltzmann-Uehling-Uhlenbeck (BUU) model, the numerical implementation of which was developed by Bauer [19], and describes the early stages of the reaction. The second is a standard statistical model, called SIMON [20], which has been modified in several respects, and models the later steps of the reaction after thermal equilibrium of the composite system is reached. Events leading to fission are tested for detection with a filter that mimics the spectrometer FOBOS and only events where the two fragments are detected are further analyzed.

The BUU model contains several features that makes it suitable for simulation of reactions in the intermediate energy domain. It can be viewed as an extension to the pure cascade model to which mean-field effects, Pauli blocking and Fermi momentum are taken into account. In the cascade model the interaction between the colliding nuclei is governed only by nucleon-nucleon collisions. This picture is valid at higher energies since Pauli blocking is essentially inexistent and the mean free path of a nucleon is hence small. At lower energies the nuclei behave in a more collective manner, nucleon-nucleon collisions are suppressed by a large Pauli blocking effect. In the intermediate energy region, viewed as a transition between the low- and high-energy extremes, both these effects are present. Hence, the BUU model describes in a way the interplay between low- and high-energy phenomena in nuclear collisions.

The numerical implementation of the BUU model by Bauer solves the transport equation,

$$\frac{\partial f}{\partial t} + \vec{v} \cdot \nabla_r f - \nabla_r U \cdot \nabla_p f = \frac{1}{(2\pi)^6} \int d^3 p_2 d^3 p_1' d^3 p_2' \sigma_{nn} v_{12} \times$$
$$\{ f f_2 (1 - f_1')(1 - f_2') - f_1' f_2' (1 - f)(1 - f_2) \} \times \delta^3 (p + p_2 - p_1' p_2') \tag{1}$$

using the parallel ensemble method in which each nucleon in the system is represented by a certain number of test particles $N$. In Eq. (1), the right-hand side is the nucleon-nucleon collision term including Pauli blocking, $\sigma_{nn}$ is the in-medium nucleon-nucleon cross section parametrized by Cugnon et al. [21], $v_{12}$ is the relative velocity of the colliding nucleons and $f(\mathbf{p}, \mathbf{r}, t)$ is the phase space distribution function of the reacting system which propagates under the influence the forces derived from the density dependent nuclear mean field potential,

$$U = A \left( \frac{\rho}{\rho_0} \right) + B \left( \frac{\rho}{\rho_0} \right)^{\sigma} \tag{2}$$

the Coulomb potential and the nucleon-nucleon collision term. The values of the parameters $A$, $B$ and $\sigma$ in Eq. (2) determine if the equation of state is "soft" or "stiff", corresponding to compressibility parameters of $K_\infty = 210$ and 380 MeV, respectively. We have used the parameters $A = -356$ MeV, $B = 303$ MeV and $\sigma = \frac{7}{6}$ describing a soft equation of state, and $\rho_0 = 0.168$ fm$^{-3}$ for the nuclear density at normal conditions. The evolution of the phase space distribution function is followed in time steps of 0.25 fm/c.

The simulations presented here are performed at energies well below the threshold for any inelastic nucleon-nucleon scattering. Hence, the production of $\Delta$-resonances and mesons is not possible and only elastic scattering occurs. Since an exchange mechanism is not modelled, we tag every particle by its identity, proton or neutron, either belonging initially to the projectile or target, the number of scatters the particle suffered during the simulation and the position $\vec{r}$ and momentum $\vec{p}$ vectors. This procedure is admittedly incorrect, but nevertheless needed in what follows to calculate several physical quantities of interest. The target-like-fragment (TLF) mass $A_{TLF}$ and charge $Z_{TLF}$ are calculated by requiring that the density of each nucleon around a volume of 1 fm$^{-3}$ (excluding its own contribution to the local density) is $\geq \frac{1}{8}\rho_0$, else the nucleon is considered unbound and treated as a pre-equilibrium particle. Particles belonging to the projectile that passed

the target without scattering with any other nucleon are considered either belonging to a projectile-like-fragment (PLF), if the average of them in all cascades is $\geq 1$, or being a pre-equilibrium particle if the above condition fails. The bound nucleons belonging to the TLF or PLF are further required to be within a sphere of radius twice the nuclear radius of the corresponding fragment. Having defined the TLF we calculate its position and momentum according to,

$$\vec{R}_{TLF} = \frac{1}{N} \sum_{i=1}^{N_{bound}} \vec{r}_i, \tag{3a}$$

$$\vec{P}_{TLF} = \sum_{i=1}^{N_{bound}} \vec{p}_i, \tag{3b}$$

where $\vec{r}_i$ and $\vec{p}_i$ are the nucleon position and momentum vectors, respectively, and the sum runs over the total number of bound TLF nucleons $N_{bound}$. We further calculate the angular momentum and excitation energy [22],

$$\vec{J}_{TLF} = \frac{1}{N} \sum_{i=1}^{N_{bound}} (\vec{r}_i \times \vec{p}_i) - \vec{R}_{TLF} \times \vec{P}_{TLF}, \tag{4a}$$

$$E^*_{TLF} = \frac{1}{N} \sum_{i=1}^{N_{bound}} \left[ \frac{\vec{p}_i^2}{2m} + \frac{e^2}{2} \sum_{j \neq i} |\vec{r}_i - \vec{r}_j|^{-1} + \frac{3}{5} E_F \left( \frac{\rho}{\rho_0} \right)^{2/3} + \frac{A}{2} \left( \frac{\rho}{\rho_0} \right) + \frac{B}{\sigma + 1} \left( \frac{\rho}{\rho_0} \right)^{\sigma} \right] - E_0, \tag{4b}$$

where he last term in Eq. (4a) is the angular momentum of the center-of-mass of the TLF about the origin, and the first term in Eq. (4b) is the contribution to the excitation energy due to the kinetic motion of the nucleons (in the center-of-mass of the TLF), the second due to the Coulomb energy between protons and the third due to the mean field potential energy. The Fermi energy $E_F$ is evaluated assuming the Fermi momentum $p_F$ of a nucleon is 0.263 GeV/c and $E_0$ is a suitable reference, taken to be the liquid drop model binding energy of a nucleus with mass $A_{TLF}$ and charge $Z_{TLF}$.

The BUU model describes rather successfully the early stages of a reaction but is unable to account for phenomena like cluster emission, statistical particle evaporation and fission. The last two are naturally better described in statistical terms with a code like SIMON. The criteria for coupling two distinct models may be important and have to be defined. In view of the limitations of BUU, we have to identify the time at which the TLF reaches thermal equilibrium and the statistical description starts to be valid. For simplicity, we have chosen to select the time when the central density of the TLF is closest to $\rho_0$ as the time when the statistical description may take over. Fig. 1 shows density profiles of the TLF in a head-on collision between $^{14}N$ and $^{197}Au$ at 53 MeV/nucleon at different simulation times. It turns out that the central density is closest to $\rho_0$ after $\sim 140$ fm/c simulation time for most impact parameters in this reaction. Accounting for the small initial time the nuclei do not interact, the formation time is of the order of $4 \times 10^{-22}$ s.

Fluctuations inherent in any quantal system are introduced numerically by Monte-Carlo sampling of the initial nucleon positions and momenta in each cascade, the nucleon-nucleon scattering angle and Pauli blocking. Since the nuclear density in a unit volume cell entering Eq. (2) is the average density of test particles in the cell and the simultaneous cascades are averaged at the end of the simulation, using a too large number of test particles per nucleon will kill the fluctuations. We have therefore used the minimum number of test particles recommended by the author ($N = 50$). To further increase the fluctuations we recourse to the trick of running a simulation several times with the same initial conditions but with different seed numbers for the random generator. A total of ten such similar simulations were ran for each impact parameter and each final TLF was coupled to the statistical code as described above.

A first series of coupled simulations for impact parameters ranging from $b = 0$ to $b = 9$ fm and the FOBOS filter indicated that the experimental linear momentum transfer is not well reproduced. We come to this conclusion by comparing the experimental and simulated fractional linear mometum transfer (FLMT) as given in the massive transfer model,

$$\text{FLMT} = \frac{v_\parallel}{v_0} \frac{1}{1 + \frac{A_p}{A_t}\left(1 - \frac{v_\parallel}{v_0}\right)} \tag{5}$$

where $v_\parallel$ is the parallel-to-the-beam recoil velocity of the TLF, deduced from the observed fission fragment velocities and angles, $v_0$ the complete fusion velocity, and $A_p$ and $A_t$ the projectile and target mass numbers, respectively. In Sec. II C it will be shown that the final state fission fragment observables and Eq. (5) gives a good estimate of the linear momentum transfer. The experimental FLMT is $\approx 0.55$, while the BUU simulations say FLMT $\approx 0.67$. To attempt a better agreement between experiment and simulation, the in-medium nucleon-nucleon cross section was reduced monotonically with density according to,

$$\sigma'_{nn} = \sigma_{nn} \times \left(1 + a\frac{\rho}{\rho_0}\right) \tag{6}$$

where $a$ is a constant, or simply by a factor $f$, $\sigma'_{nn} = \sigma_{nn} \times f$. Fig. 2 shows the properties of the TLF as a function of simulation time for impact parameter $b = 5$ fm, using $f = 1.0$ (solid lines), $f = 0.8$ (dashed lines) and $a = -0.2$ (dotted lines). Panel a) displays the mass of the TLF, panel b) the fractional linear momentum transferred to the TLF, panel c) the transferred angular momentum perpendicular to the reaction plane, panel d) the ratio of TLF excitation energy to the excitation energy assuming complete fusion of projectile and target, panel e) the number of unbound charged particles and panel f) the central density ($r \leq 3$ fm) of the TLF. As seen $f = 0.8$ gives a straightforward reduction of most quantities while $a = -0.2$ has a bit different functional form than the $f = 1.0$ case. The reduction $a = -0.2$ gives slightly higher momentum transfer after $\sim 120$ fm/c, and since this is the quantity we wanted to reduce, we choose the reduction $f = 0.8$ in forthcoming simulations. The excitation energy oscillates quite markedly during expansion or compression periods, and is near a turning point of maximum excitation energy after $\sim 130$ fm/c in the $f = 1.0, 0.8$ cases and $\sim 120$ fm/c in the $a = -0.2$ case. Fig. 3 shows the same properties of the TLF as a function of $b$ after 140 fm/c for the $f = 0.8$ case, and after 130 fm/c for the $a = -0.2$ case. The mass of the TLF and the

6

excitation energy are lower in the former case mostly because they are taken 10 fm/c after the latter case.

## B. The statistical evaporation model

The properties of the TLF $(A, Z, \vec{P}, \vec{J}, E^*)$ derived from the BUU simulations served as input for the statistical model code SIMON [20]. This code was primarily developed for the statistical description of the multifragment decay of a hot nucleus. We have made several changes to better describe the fission process. The emission of light particles and clusters with $Z \leq 4$ and $A \leq 8$ are allowed to compete with fission. For each possible decay,

$$(A_0, Z_0) \longrightarrow (A_1, Z_1) + (A_2, Z_2) \tag{7}$$

where the subscript 0, 1 and 2 refer to the decaying nucleus, the emitted particle and the daughter nucleus, respectively, the statistical decay width is calculated. In the case of light-particle and cluster emission the decay width is given by [23,24],

$$\Gamma_i^n = T_{12} \frac{kA_1^{-p} \times kA_2^{-p}}{kA_0^{-p}} \sqrt{4\pi T_{12} E_{12}^*} \exp\left[2\sqrt{a_1 E_1^*} + 2\sqrt{a_2 E_2^*} - 2\sqrt{a_0 E_0^*}\right] \tag{8}$$

where $T$ is the nuclear temperature, $E^*$ the thermal excitation energy, $a$ the level density parameter, $k = 0.2$ MeV$^{-1}$, $p = \frac{5}{3}$ and the subscript 12 refers to the "activated complex" at the barrier. This decay width is not appropriate for the description of fission because it depends on properties of the fragments at infinite separation, contradicting the standard transition-state hypothesis. In the case of fission $(A_1 > 8, Z_1 > 4)$ we therefore use,

$$\Gamma_i^f = T_{12}\sqrt{\frac{a_{12}}{a_0}} \left(\frac{E_{12}^r}{E_0^r}\right)^{\frac{3}{2}} \left(\frac{E_0^* - E_0^r}{E_0^* - B - E_{12}^r}\right)^2 \exp\left[2\sqrt{a_{12}\left(E_0^* - B - E_{12}^r\right)} - 2\sqrt{a_0\left(E_0^* - E_0^r\right)}\right] \tag{9}$$

where $E^*$ is the excitation energy, $E^r$ the rotational energy, $B$ the fission barrier and the subscript 12 now refers to the saddle point. Temperature dependent level densities are calculated with the analytical expressions of Lestone [25], fission barriers with the formalism described in the Appendix A of Ref. [23], and ground state $Q$-values with a standard compilation of mass excesses [14]. Furthermore, because of deformation, we assume the level density at the saddle point relative to the ground state is increased by $a_{12} = 1.02a_0$. The other important ingredient in Eq. (9) are the rotational energies. These are evaluated using standard liquid drop formulae, assuming a rigid sphere in the case of the ground state and two touching rigid spheres with the centers-of-mass separated by $R_1 + R_2 + 2$ fm in the case of the saddle point.

The effect of retardation is introduced by reducing the fission decay width Eq. (9),

$$\Gamma_i^f(t) = \Gamma_i^f \left(\sqrt{1 + \gamma^2} - \gamma\right) \left[1 - \exp\left(\ln(0.1)\frac{t}{\tau}\right)\right] \tag{10}$$

where $\gamma$ is the nuclear friction coefficient and $\tau$ is the transient time needed for the fission probability flow to build up inside the barrier [26] and parametrized according to [9],

$$\tau = \frac{1}{2\gamma}\ln\left(\frac{10B}{T}\right) + 0.0112\frac{\gamma A}{T} \tag{11}$$

In each cascade the total width $\Gamma_{tot} = \sum \Gamma_i$ is calculated and a particular decay $j$ is selected by the condition,

$$R\Gamma_{tot} \leq \sum_{i=1}^{j} \Gamma_i \tag{12}$$

where $R$ is a random number. The emission time is calculated by,

$$t_e = -\frac{\hbar}{\Gamma_{tot}}\ln(R) \tag{13}$$

in the same manner as done by Gavron [1], and the cumulative time $t_c$ is the sum of the emission times of the decay and all previous decays, $t_c = \sum t_e$. If the decaying nucleus is committed to fission, we further calculate the saddle-to-scission time [27],

$$t_{ssc} = t_{ssc}^0\left(\sqrt{1+\gamma^2} + \gamma\right) \tag{14}$$

where $t_{ssc}^0$ is the saddle-to-scission time in the absence of dissipation and evaluated by assuming the scission point consist of two rigid spheres separated by a distance consistent with the total kinetic energy of the fragments [7],

$$\text{TKE} = 0.755\frac{Z_1 Z_2}{A_1^{1/3} + A_2^{1/3}} + 7.3 \text{ MeV} \tag{15}$$

and static potential energies given by liquid drop model expressions. For Au-like nuclei we estimate $t_{ssc}^0 \approx 2.6 \times 10^{-21}$ s and $t_{ssc}^0 \approx 2.2 \times 10^{-21}$ s for symmetric and very asymmetric mass divisions, respectively. The cumulative time in the case of fission is then taken as $t_c = \sum t_e + t_{ssc}$. In this way we include the transient time of fission correctly, but elude to model the near scission emission of particles in view of the lack of knowledge about this intricate emission process.

The "real" time $t$ is followed through suitable time steps $\Delta t$ starting from $t = 0$ fm/c. Once a decay is selected by condition Eq. (12) the decaying nucleus is "inert" for decay if $t < t_c$, meanwhile the trajectories of all particles are followed and corrected for Coulomb repulsion. When $t \geq t_c$ the decaying nucleus split and the fragments become "active" for decay again. The cascades are followed until the total energy is less that 20 MeV or $t > t_{max}$ (selected internally).

### C. Comparison between experiment and simulation

The $4\pi$ spectrometer FOBOS consists of six rings of five modules each, with angles listed in Table 1 of Ref [18]. The experimental filter to the simulated events takes into account this geometry. The reaction plane of each event is rotated randomly several times and the direction of every particle in the event is tested whether it can be detected by one module in each case. This generates several patterns of detection. We further consider only events where the two fission fragments are detected, and only one of those patterns is selected randomly and further analyzed.

We run 10000 cascades for each TLF resulting form the BUU simulations, and since we run, for each impact parameter, ten BUU simulations with different seed number for the random generator, we run a total of 1000000 cascades. In Fig. 4a we show the simulated fission probability $P_f$ as a function of impact parameter for two cases, with $\gamma = 1$ and $\gamma = 3$, respectively. The fission probability is constructed by counting the number of fission events and weighting by the partial cross section $d\sigma = 2\pi b d\sigma$ of the impact parameter. The rapid increase with impact parameter is naturally connected with the increase of angular momentum to the composite system with the same quantity (cf. Fig. 3c) and the corresponding decrease of the fission barrier. The total fission probability $\sigma_F/(\sigma_F + \sigma_{HR})$ amounts to $\sim 38\%$ in the $\gamma = 1$ case, and to $\sim 24\%$ in the $\gamma = 3$ case. Similarly, a simulation with $\gamma = 4$ gives a total fission probability $\sim 10\%$. The experimental fission probability for this system is estimated to $\sigma_F/(\sigma_F + \sigma_{HR}) \sim 25\%$ by interpolating the data of Sonzogni et al. [28], arguing for an overdamped fission motion consistent with $\gamma \approx 3$. In Fig. 4b we show the fission time as a function of impact parameter in the case of $\gamma = 3$. The error bar is the standard deviation of the ten simulations for each impact parameter. The fission time also follows a trend consistent with the decrease and increase of the fission barrier with angular momentum given to the TLF. The mean time from formation of the TLF to the time of scission, $t_f(b)$ weighted by $P_f(b)$, is $(28 \pm 6) \times 10^{-21}$ s.

In what follows we select fission fragment events triggered by the first and fourth FOBOS ring (condition a), events triggered by the first and sixth rings (condition b), and require linearity in the azimuthal. The former combination of detectors have the smallest possible folding angle, selecting on average the most central events.

Fig. 5 shows a comparison between the experimental and simulated distributions of the folding and coplanarity angles, assuming $f = 0.8$, $\gamma = 3$ and taking the events in condition a. The simulated folding angle peaks closely to the experimental value. The width is however not reproduced arguing for a lack of fluctuations in BUU. Assuming the massive transfer model and that the recoil velocity of the compound nucleus parallel to the beam is given by the observed fragment velocities and angles gives FLMT$\approx 0.60$, while the mean FLMT in the BUU simulations is FLMT$\approx 0.59$, if weigthing by the number of events and the partial cross section for each impact parameter. This shows that the massive transfer model gives a rather good estimate of FLMT from fission fragment final state observables. Making the same assumptions as above to the experimental data gives FLMT$\approx 0.55$, which deviates a bit from simulation, although we match the folding angle distribution to precision for condition a (cf. Fig. 5a). This indicates that relying only on the folding angle distribution may be deceitful as the distribution depends on detector geometry considerably.

Neither the width of the coplanarity angle is reproduced, but the mismatch here seems to be a consequence of too low transversal momentum components given to the composite system in BUU. The width of the coplanarity angle is not strongly dependent on the recoils experienced by the compound nucleus and fragments due to particle evaporation. The width is only slightly increased assuming $\gamma = 1$, although the multiplicities of evaporated particles from the compound nucleus and fragmements are quite different. To demonstrate this, we artificially increased the transversal momenrum components by as much as 60%, giving a width consitent with experiment. The transversal velocity is roughly reproduced by this artificial increase.

The initial excitation energy in the massive transfer model [29], on the other hand, is

a bit less transparent to deduce since it depends critically on the ground state Q-value of the assumed incomplete fusion fragmentation. We can match the initial excitation energy in BUU to that given by the massive transfer model by assuming the fragmentation $^{14}$N$+^{197}$Au$\longrightarrow ^{197}$Au$+^4$He$+5$n$+5$p on average occurs. Applying these criteria to the experimental data we arrive to the conclusion that the composite systems are formed with nuclear temperatures $T \sim 4$ MeV. These exercises naturally help in deducing FLMT, excitation energies and other quantities when analyzing experimental data.

In Fig. 6a we show the experimental and simulated mass distributions. The mean in the mass distribution, as well as its width, are rather well reproduced. The yield of very asymmetric splits is however underestimated probably in part, because of a contamination of heavy residues and intermediate mass fragments in the experimental data. Panels b) and c) give the TKE distributions in logarithmic scale. In Fig. 7 we plot the mean and the width of the TKE distribution as a function of the lighter fragment mass. The simulations are rather successful in describing the mean TKE of fission for the more symmetric mass splits by randomly choosing the fraction of thermal energy left for kinetic motion consistent with a Maxwell distribution. The dotted line shows the prediction of Eq. (15) assuming the compound nucleus is $^{197}$Au, and the dashed lines shows the prediction of a recent parametrization [30],

$$\text{TKE} = 0.29 \frac{Z^2}{A_1^{1/3} + A_2^{1/3} - A^{1/3}} \times \frac{A_1 A_2}{A^2} \text{ MeV} \tag{16}$$

assuming the fissioning system is $^{176}$Ir, which is the average compound nucleus derived from the experimental masses and charges of the fission fragments. The FWHM of the TKE distribution is not reproduced, probably as a consequence of the lack of fluctuations in BUU. Its increase with mass asymmetry in the experimental case indicates that the fissioning system has on average more excitation energy at the moment of scission in asymmetric splits, since the width in the kinetic energy distributions is $\propto (E_1^* + E_2^*)^{1/4}$. This is consistent with a faster time scale for asymmetric mass splits; nuclear matter needs less rearrangement in this case, hence the shorter time scale.

## III. MOVING SOURCE FITTING

The energy and angular distributions of light charged particles bear distinct features of their source of emission. In particular, they are kinematically focused along the direction of motion of the source. In the case of light charge particles, the mean kinetic energy is strongly connected with the mean emission barrier and the slope of the distribution at higher energies with the temperature of the source. It is therefore possible to separate their relative yield by fitting the distributions with a moving source parametrization.

### A. Pre- and post-scission evaporation particles

The code CPE [31] performs such a fitting by assuming the kinetic energy distributions of light charged particles emitted from the compound nucleus and the fission fragments, in their respective rest frames, have a Maxwellian form,

$$N(\epsilon) = 0, \text{ if } \epsilon \leq B', \tag{17a}$$

$$N(\epsilon) \propto C'\left(\epsilon - B'\right)^D \exp\left(-\frac{\epsilon}{T}\right), \text{ if } B' < \epsilon < B + T, \tag{17b}$$

$$N(\epsilon) \propto (\epsilon - B) \exp\left(-\frac{\epsilon}{T}\right), \text{ if } \epsilon \geq B + T, \tag{17c}$$

where $C' = T/(DT)^D$ and $B' = (1 - D)T + B$. The parameter $T$ is the mean temperature of the source and controls the slope of the energy distribution at higher energies, $B$ the mean height of the emission barrier, and $D$ is related to the curvature and penetrability of the barrier and controls the slope of the distribution at lower energies. The maximum of the distribution occurs at $B + T$. The parameter $D$ depends in a complicated manner on the distribution of barriers. We therefore regard $D$ as a parameter simply, without making physical interpretations. The emission from the compound nucleus is naturally considered pre-scission and the energy distribution of light charged particles in its rest frame assumes the form Eq. (17) with parameters $D_{CN}$, $T_{CN}$ and $B_{CN}$. Similarly, the post-scission emission from the heavier and lighter fission fragments are described by parameters $D_{FH}$, $T_{FH}$, $B_{FH}$, and $D_{FL}$, $T_{FL}$, $B_{FL}$, respectively.

The near-scission emission is further assumed to have independent Gaussian kinetic energy and angular distributions in the rest frame of the compound nucleus,

$$N_{nse}(\epsilon) \propto \exp\left[-\frac{(\epsilon - \bar{\epsilon})^2}{2\sigma_\epsilon^2}\right], \tag{18a}$$

$$W_{nse}(\phi_{sc}) \propto \exp\left[-\frac{(90° - \phi_{sc})^2}{2\sigma_{sc}^2}\right], \tag{18b}$$

where $\bar{\epsilon}$ and $\sigma_\epsilon$ are the mean and standard deviations of the kinetic energy distribution, $\phi_{sc}$ is the angle of emission relative the scission axis and $\sigma_{sc}$ the standard deviation of the angular distribution. Although we do not simulate near scission emission and do not include such an emission source in what follows, we mention it because of completeness.

The code CPE constructs energy distributions in the rest frame of the compound nucleus according to parametrizations Eqs. (17) and (18), and energy distributions in the rest frame of the fission fragments according to parametrization Eq. (17). Further, each distribution is properly normalized $\int N(\epsilon)d\epsilon = 1$ and the distributions at different selected angles $\theta_i$ in a common frame are constructed by making transformations dependent on the direction of motion and velocity of the sources in the frame relative the angle of observation. The total particle spectrum in one such angle of observation in the common frame is then,

$$N_{tot}(\epsilon, \theta_i) = \mu_{CN}N_{CN}(\epsilon, \theta_i) + \mu_{nse}N_{nse}(\epsilon, \theta_i) + \mu_{FH}N_{FH}(\epsilon, \theta_i) + \mu_{FL}N_{FL}(\epsilon, \theta_i) \tag{19}$$

where the normalization constants $\mu_{CN}$, $\mu_{nse}$, $\mu_{FH}$ and $\mu_{FL}$ are the multiplicities from compound nucleus, near-scission, heavier and lighter fission fragment emission, respectively. The parameters and normalization constants are then varied to simultaneously fit the experimental kinetic energy distributions at the same angles of observation by minimizing the $\chi^2$,

$$\chi^2 = \sum_i \sum_\epsilon \left[ \frac{N_{exp}(\epsilon, \theta_i) - N_{tot}(\epsilon, \theta_i)}{\Delta N_{exp}(\epsilon, \theta_i)} \right]^2 \tag{20}$$

where $N_{exp}(\epsilon, \theta_i)$ is the experimental distribution and $N_{exp}(\epsilon, \theta_i)$ its error.

### B. Pre-equilibrium particles

In reactions near and above the Fermi energy the multiplicity of pre-equilibrium light charged particles is high. In any attempt to extract multiplicities one therefore needs to take these particles into account as they may contaminate the pure evaporation components considerable. We have assumed the energy spectra of pre-equilibrium particles in the center-of-mass of their source have the shape of Eq. (17), or the shape,

$$N(\epsilon) \propto \frac{1}{T^{\frac{3}{2}}} (\epsilon - B)^{\frac{1}{2}} \exp\left(-\frac{\epsilon - B}{T}\right) \tag{21}$$

appropriate for volume emission, and that the velocity of the source is directed along the beam axis. In order to test the above assumptions, we have used the BUU simulations. Since BUU is unable to account for cluster formation, we can only construct energy distributions of pre-equilibrium protons. The immediate problem that arises is that pre-equilibrium particles have no definite source. In the BUU simulations, some projectile nucleons may pass the target without colliding with any nucleon. These particles would then have velocities close to the beam velocity and would barely be deflected from the beam axis. Other projectile nucleons may scatter some few times and then be emitted before the composite system reaches thermal equilibrium. Furthermore, some target nucleons may also be given considerable momentum to escape from the forming composite system. One may therefore expect a whole range of source velocities. In view of this we consider the velocity of the pre-equilibrium source as a parameter.

A first attempt to fit the energy distributions of the simulated pre-equilibrium particles assuming only one source of emission failed completely. However, a second attempt assuming instead two sources was convincingly successful. In Fig. 8 we show a fit to constructed energy distributions, from $\theta_{lab} = 5° - 155°$ in 15° steps, of simulated pre-equilibrium protons. The first source is very fast with $\sim 70\%$ of the beam velocity, and the second is slower with $\sim 25\%$ of the beam velocity. The yield of the fast source is naturally dominant at forward angles because of the kinematical focusing, while the slower source grows successively in importance relative the fast source as the angle to the beam increases, as a consequence of the reduced focusing effect. The fitted temperatures are similar for both sources $T \sim 10$ MeV with no appreciable barrier. Using the parametrization Eqs. (17) and (21) or combinations of both for the two sources give essentially the same result. Taking the mean, the extracted total multiplicity is 5.3, to be compared with the true multiplicity of 5.5 protons per event. Although the total and partial multiplicities of the two sources most certainly do not coincide with experiment because of the limitations of the BUU model, we may draw the conclusion that in order to extract the light charged particle multiplicities we need to consider at least two pre-equilibrium sources, one with very high velocity associated with projectile nucleons or fragments, and the other with a slower source velocity associated with nucleons or clusters emitted from the forming composite system before full thermal equilibrium is reached.

12

## C. Construction of total energy distributions

Having established how to treat the pre-equilibrium multiplicity components we now use the full set of light charged particles by combining the pre-equilibrium particles generated by the BUU simulations and those generated in the statistical model. We include randomly 50% of the pre-equilibrium particles generated in the cascades in BUU into the evaporation events. We do so because the yield of true pre-equilibrium protons should be less than the yield of pre-equilibrium charged test particles in BUU.

The moving source fitting requires well-defined sources. Since FOBOS is able to assign masses and linear momentum components of the fission fragments we construct light charged particle energy distributions depending on the direction and mass of the fission fragments. To further exploit the advantages of FOBOS, we construct the energy distributions in the rest frame of the compound nucleus, event by event. In this frame we need only to consider the angle of the particle relative the scission axis, needed to fit the post-scission components, and the angle relative the beam axis, needed to fit the pre-equilibrium components. We further use the mean velocities of the fission fragments as source velocities. In Fig. 9 we show such energy distributions of protons constructed by requiring the heavier fission fragment to be detected in the first FOBOS ring and the lighter fission fragment in the fourth ring. Because of fission kinematics, this condition selects on average the most central collisions. A simultaneous fit to the energy distributions was done assuming two pre-equilibrium sources, directed along the beam-line with unknown source velocities, one compound nucleus source and two post-scission sources with defined directions and velocities, as described above. Hence, a total of 17 fit parameters are considered, 9 describing the evaporation spectra and 8 the pre-equilibrium spectra. The fitted components are shown as solid colored lines. The red line labeled CN corresponds to the compound nucleus source, the green line labeled FH to the heavier fission fragment, the blue line labeled FL to the lighter fission fragment, the cyan line labeled PQ1 to the slower pre-equilibrium source, and the magenta line labeled PQ2 to the faster pre-equilibrium source, respectively. We hope the reader appreciates the quality of the fit, despite the large number of sources considered with the corresponding large number of fitting parameters. The multiplicities in this simultaneous fit are well reproduced, and given in Table I together with the true mean multiplicities. In Table II we give the fitted parameters $T$ and $B$ and the mean temperatures and barriers at the moment of emission for the evaporation components. As seen, the fitted parameters are rather representatives of their physical counterparts as well.

The most striking feature of Fig. 9 is that the slower pre-equilibrium source yield at the most backward angles $\theta \sim 145°$ (modules 26-30) is very high. Hence, the simulations and the fit to the constructed energy spectra of protons seem to suggest that one cannot in general tackle the question about pre-equilibrium emission in incomplete fusion-fission reactions by just regarding the emission of particles in the backward direction as purely evaporative, as normally done in complete fusion-fission reactions.

## IV. CONCLUSIONS

In fitting kinetic energy distributions of protons at different angles, constructed with realistic simulations, we come to the conclusion that in order to reproduce successfully the

distributions one needs to consider at least two pre-equilibrium sources, one with velocity comparable to that of the beam and the other with considerable less velocity. The two distinct moving sources have nevertheless characteristic pre-equilibrium features, i.e. high temperatures and vanishing barriers. In the BUU simulations the former arises mostly from projectile particles that did not collide with any other nucleon during the simulation, hence its apparent high source velocity, while the latter can be associated with projectile as well as target particles that scatter a few times and are then emitted before one can assume full thermal equilibrium of the forming composite system is reached. Although we cannot assign much credit to the total and partial multiplicities of the simulated pre-equilibrium protons, we recognize that the yield of the slower pre-equilibrium source at the most backward angle could be substantial and of the order of the evaporative components. Moreover, since the pre-equilibrium particle emission seems to saturate after $\sim$ 120 fm/c simulation time (cf. Fig. 2e) and the mean time of emission of the first proton in the statistical model simulation is $\sim$ 100 fm/c, it seem feasible that the two distinct sources (slower pre-equlibrium and equilibrated compound nucleus) are well distinguished in experiment too, judging from the very distinct set of parameters needed to fit their spectra.

In summary, we have demonstrated the need and the feasibility of including pre-equilibrium sources in conventional moving source analyses when attempting to extract pre- and post-scission multiplicities in incomplete fusion-fission reactions.

[1] A. Gavron et al., Phys. Rev. C **35**, 579 (1987).
[2] J.O. Newton et al., Nucl. Phys. **A483**, 126 (1988).
[3] D.J. Hinde et al., Phys. Rev. C **45**, 1229 (1992).
[4] J.P. Lestone et al., Nucl. Phys. **A559**, 277 (1993).
[5] I. Diôszegi et al., Phys. Rev. C **46**, 627 (1992).
[6] P. Paul, M. Thoennessen, Ann. Rev. Nucl. Part. Sci. 44, 65 (1994).
[7] V.E. Viola et al., Phys. Rev. C **31**, 1550 (1985).
[8] J.P. Lestone, Phys. Rev. Lett. **70**, 2245 (1993).
[9] G. van't Hof et al., Phys. Rev. C **54**, R1515 (1996).
[10] K. Siwek-Wilczyñska et al., Phys. Rev. C **51**, 2054 (1995).
[11] N. Bohr, J.A. Wheeler, Phys. Rev. **56**, 426 (1939).
[12] H.A. Kramers, Physica **7**, 284 (1940).
[13] H. Ikezoe et al., Phys. Rev. C **42**, 342 (1990);
    H. Ikezoe et al., Phys. Rev. C **42**, R1187 (1990);
    H. Ikezoe et al., Nucl. Phys. **A538**, 299c (1992).
[14] A. Gavron, Phys. Rev. C **21**, 230 (1980).
[15] D.J. Hofman et al., Phys. Rev. C **51**, 2597 (1995).
[16] L.G. Moretto et al., Phys. Rev. Lett.**75**, 4186 (1995).
[17] P. Fröbrich et al., Nucl. Phys. **A556**, 281 (1993).
[18] H.-G. Ortlepp et al., to be published in Nucl. Instr. and Meth. A (May 1997).
[19] W. Bauer, Phys. Rev. C **40**, 715 (1989).
[20] D. Durand, Private communication.
[21] J. Cugnon et al., Nucl. Phys. **A352**, 505 (1981).
[22] B.M. Heidel, Doctoral Thesis, FZR-108 (1995).
[23] J. Lopez, J. Randrup, Nucl. Phys. **A503**, 183 (1989).
[24] J. Lopez, J. Randrup, Nucl. Phys. **A512**, 345 (1990).
[25] J.P. Lestone, Phys. Rev. C **52**, 1118 (1995).
[26] P. Grange et al., Phys. Rev. C **34**, 209 (1986).

[27] H. Hofmann, J.R. Nix, Phys. Lett. **122B**, 117 (1983).

[28] A. Sonzogni et al., Phys. Rev. C **53**, 243 (1996).

[29] E. Mordhorst et al., Phys. Rev. C **43**, 716 (1991).

[30] W. Wagner, H.-G. Ortlepp, Forshungszentrum Rossendorf Annual Report 1996, FZR-**179** (1997).

[31] J.P. Lestone, Doctoral Thesis, Australian National University (1990).

TABLE I. Fitted and true mean multiplicities.

| Source | Fitted multiplicity | True multiplicity |
|---|---|---|
| CN | 0.385 | 0.384 |
| FH | 0.202 | 0.192 |
| FL | 0.086 | 0.101 |
| PQ[a] | 3.485 | 3.592 |

[a]The two pre-equilibrium source multiplicities are summed together.

TABLE II. Fitted parameters $T$ and $B$ and mean temperature of the sources and barriers at the moment of emission.

| Source | $T$ (MeV) | Temperature (MeV) | $B$ (MeV) | Barrier (MeV) |
|---|---|---|---|---|
| CN | 3.9 | 3.4 | 8.8 | 9.5 |
| FH | 2.6 | 2.0 | 6.7 | 6.3 |
| FL | 1.9 | 2.0 | 6.7 | 4.9 |

## FIGURE CAPTIONS

**Fig.1** Density profiles of TLFs for impact parameter $b = 0$ fm as a function of simulation time.

**Fig.2** Properties of TLFs for $b = 5$ fm as a function of simulation time. a) mass of the TLF, b) FLMT, c) transferred angular momentum, d) excitation energy, e) number of unbound charged particles and f) central density. Results with a reduced in-medium cross section are shown in solid lines, those not reduced in dashed lines.

**Fig.3** Properties of TLFs after 140 fm/c simulation time as a function of impact parameter. a) mass of the TLF, b) FLMT, c) transferred angular momentum, d) excitation energy, e) number of unbound charged particles and f) central density.

**Fig.4** a) Simulated fission probability b) mean fission time as a function of impact parameter $b$.

**Fig.5** Comparison between experimental and simulated distributions of the a) folding and b) coplanarity angles in binary fission events.

**Fig.6** Experimental and simulated distributions of a) fragment mass, and b) and c) TKE.

**Fig.7** Experimental and simulated a) mean TKE and b) width of TKE distribution as a function of the lighter fragment mass.

**Fig.8** Fit to simulated pre-equilibrium proton energy distributions assuming two sources of emission.

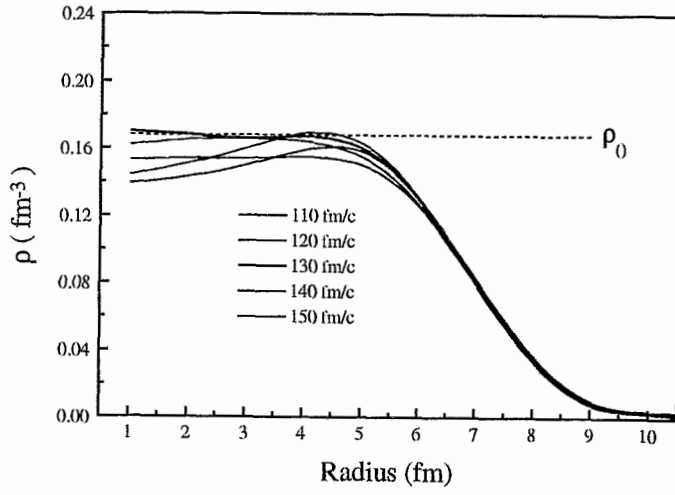**Fig.9** Fit to simulated proton energy distributions assuming two pre-equilibrium source, one pre-scission and two post-scission sources.
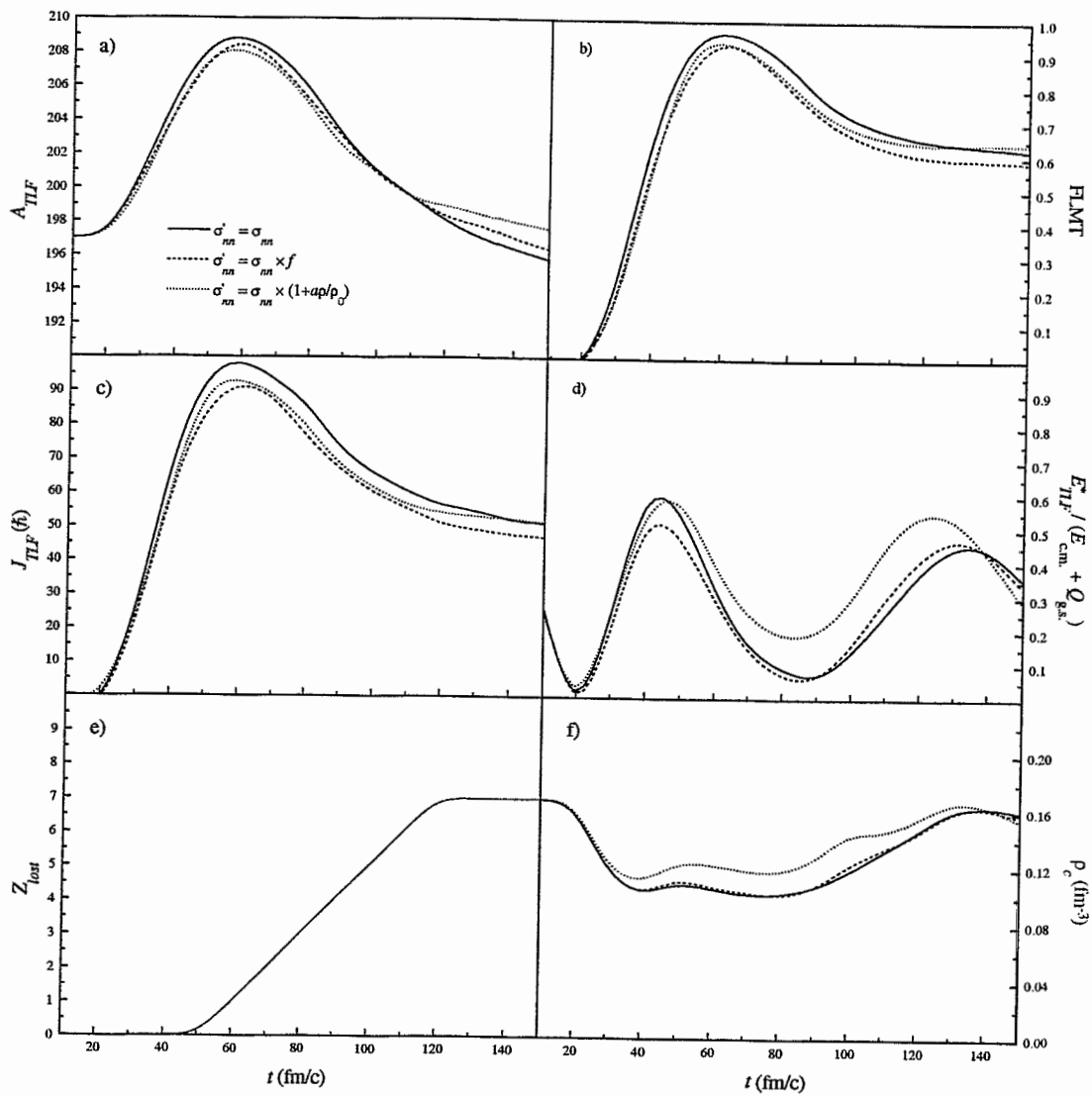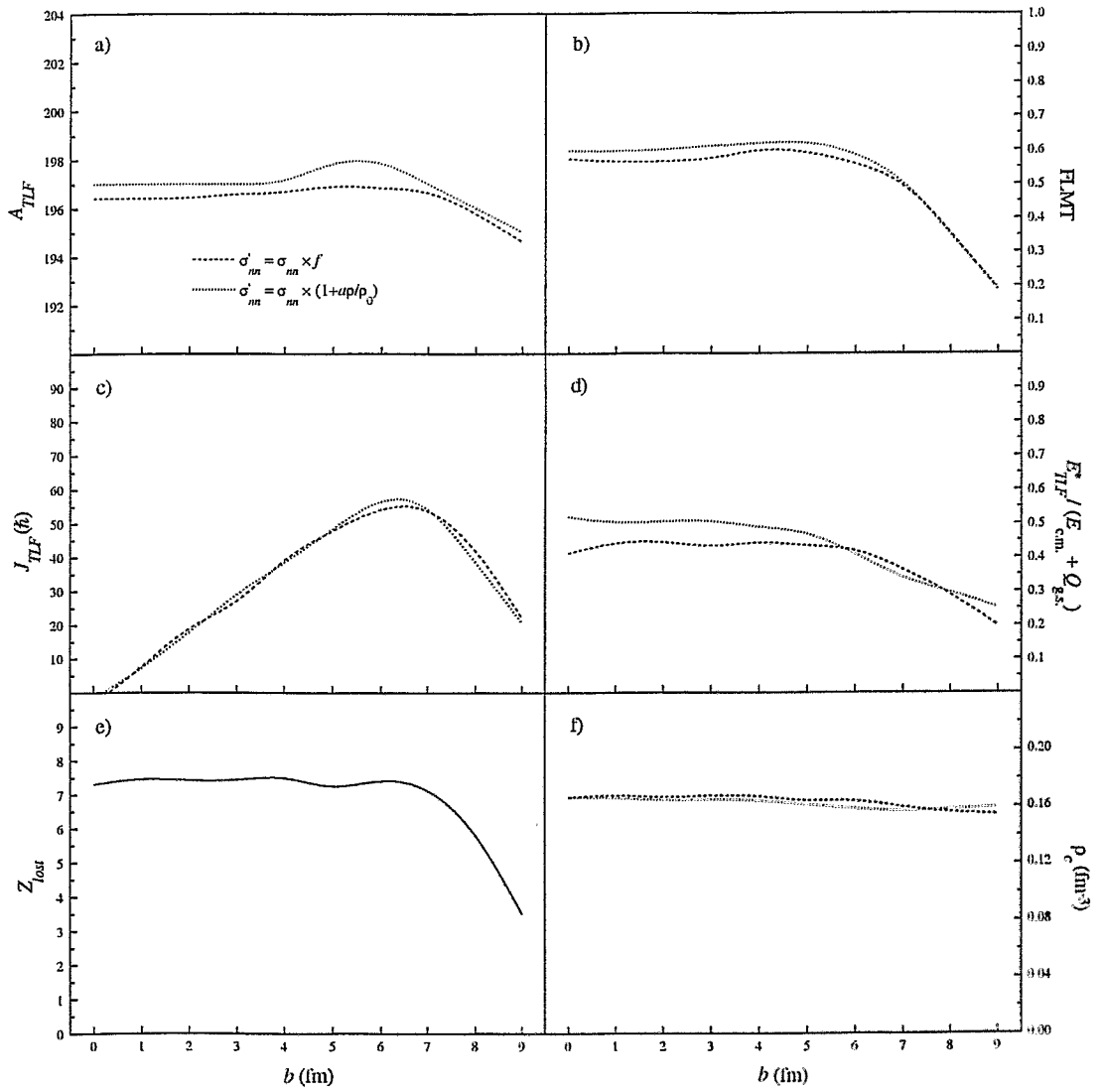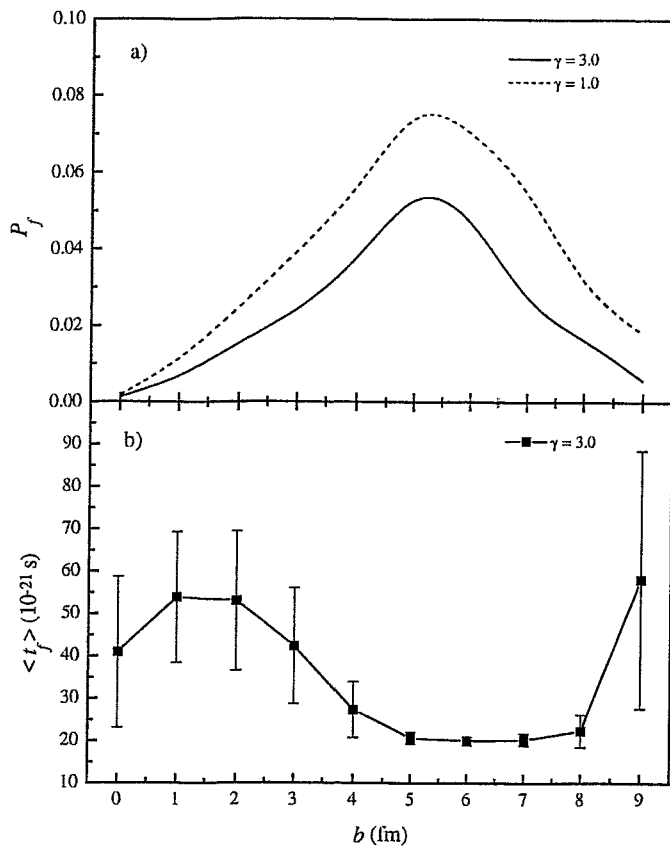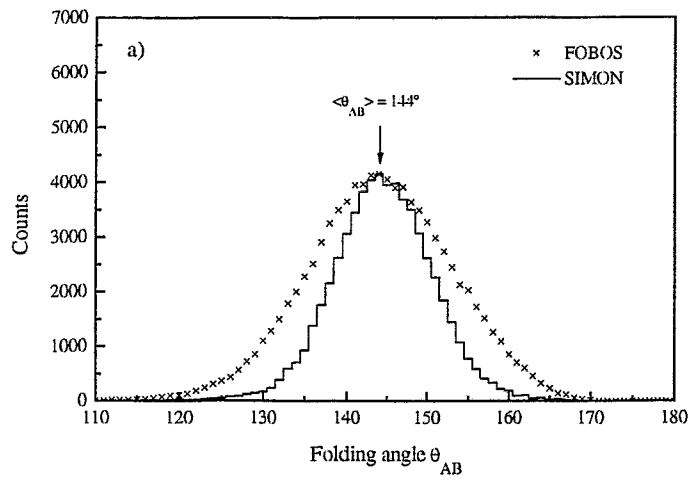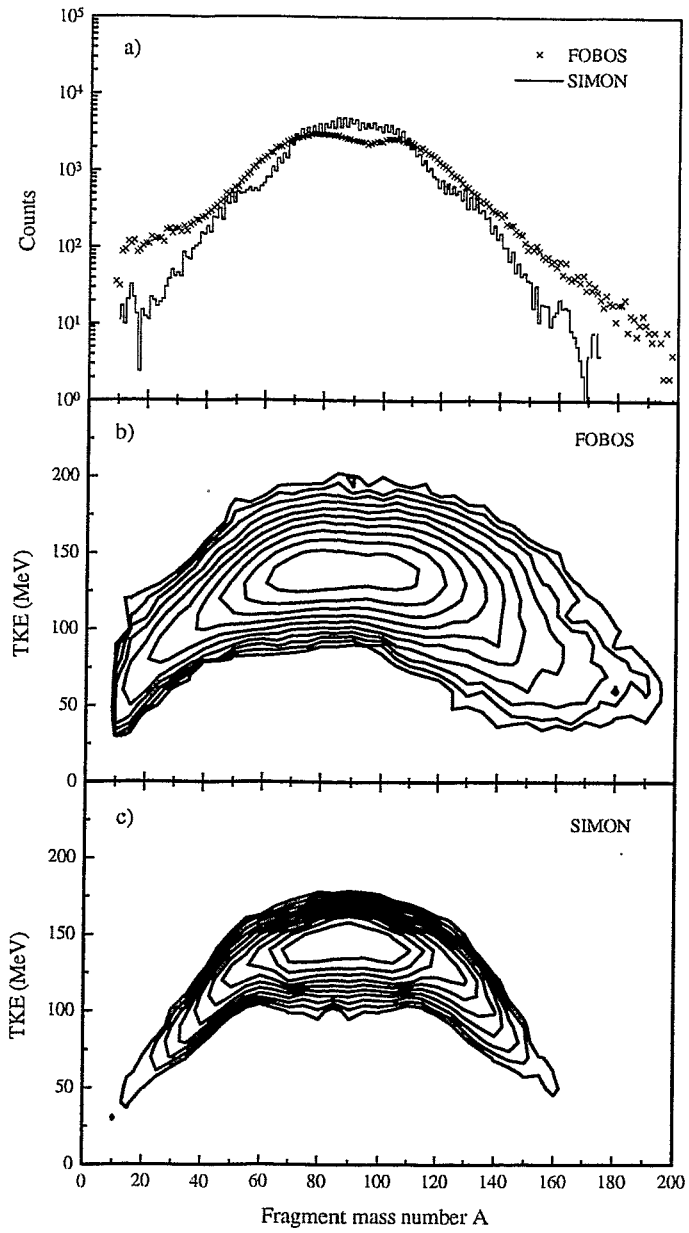
Fig. 1

Fig. 2

Fig. 3

Fig. 4
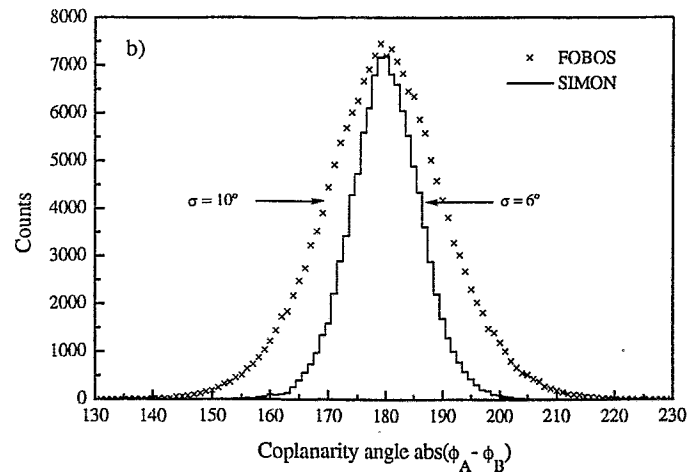
Fig. 5

Fig. 6

Fig. 7

Fig. 8

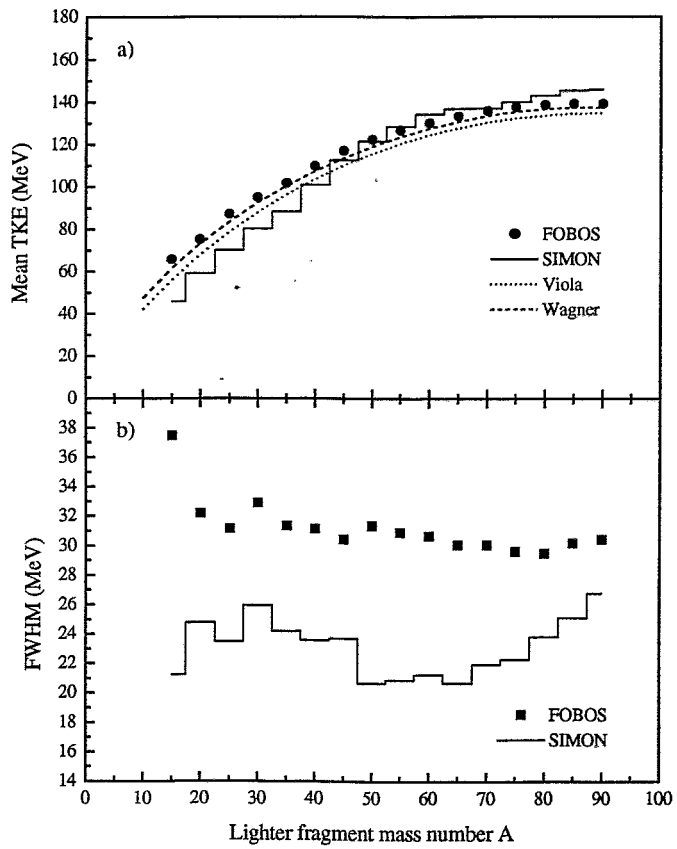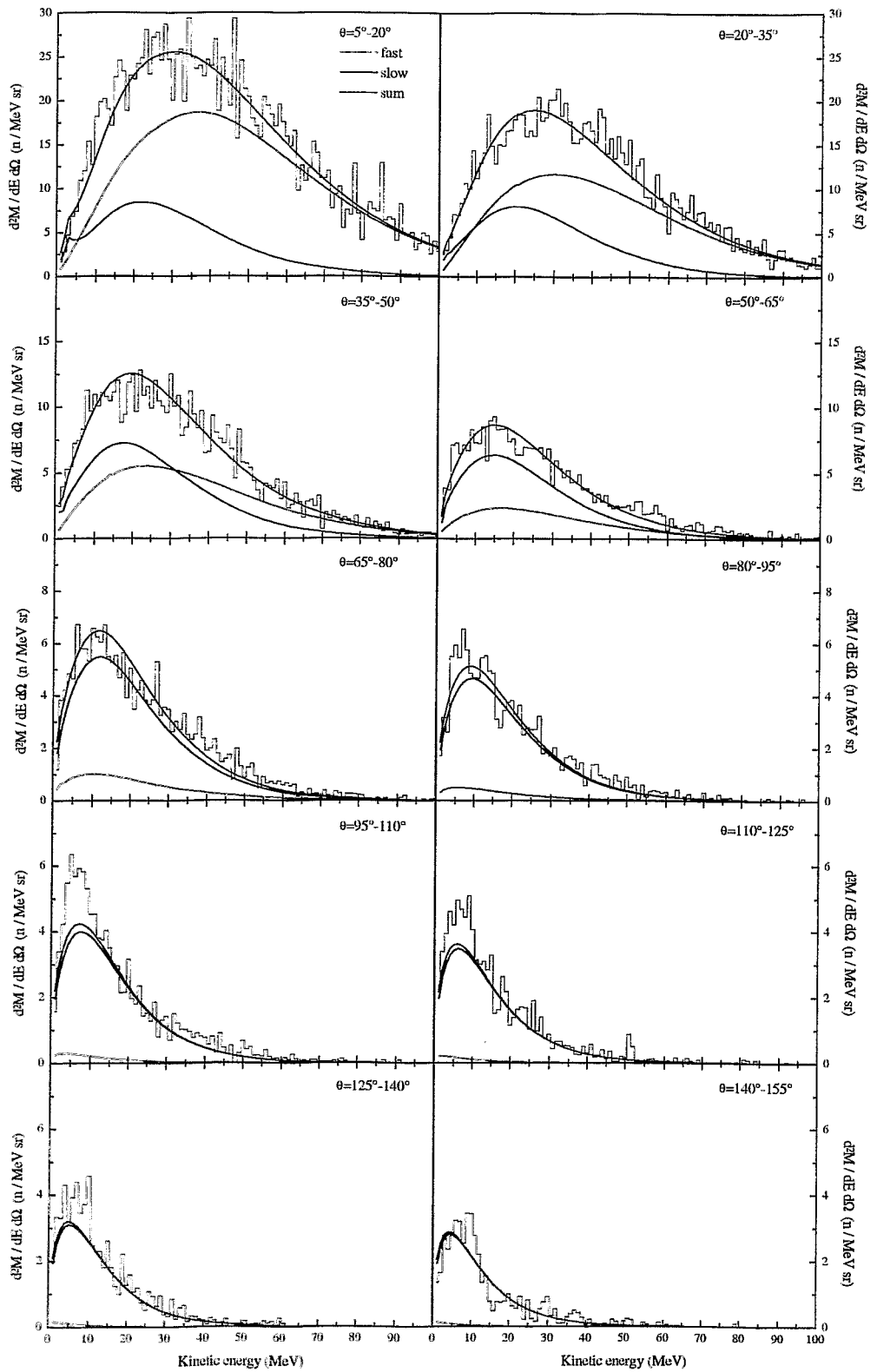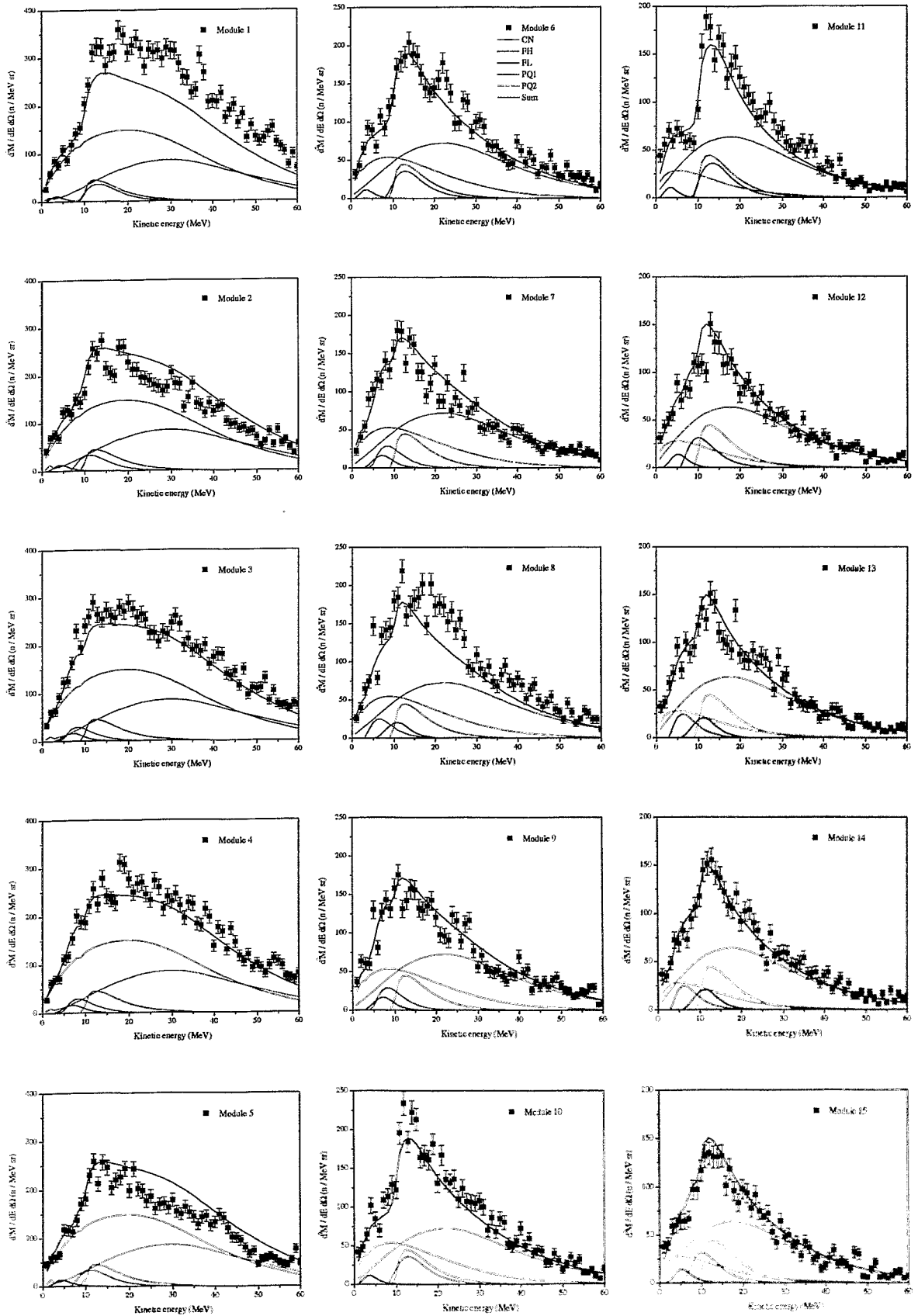# proton cm spectra (simulation)
## Modules 1-15



Fig. 9a

# proton cm spectra (simulation)
## Modules 16-30



Fig. 9b